Journal of Hazardous Materials 186 (2011) 1445–1454

Contents lists available at ScienceDirect

Journal of Hazardous Materials

journal homepage: www.elsevier.com/locate/jhazmat

Synthesis and physicochemical characterizations of nanostructured $Pt/Al_2O_3–CeO_2$ catalysts for total oxidation of VOCs

Zahra Abbasi[a,b], Mohammad Haghighi[a,b,c,*], Esmaeil Fatehifar[a,b,c], Saeed Saedy[a,b]

[a] Chemical Engineering Department, Sahand University of Technology, P.O. Box 51335-1996, Sahand New Town, Tabriz, Iran
[b] Reactor and Catalysis Research Center (RCRC), Sahand University of Technology, P.O. Box 51335-1996, Sahand New Town, Tabriz, Iran
[c] Environmental Engineering Research Center (EERC), Sahand University of Technology, P.O. Box 51335-1996, Sahand New Town, Tabriz, Iran

ARTICLE INFO

Article history:
Received 12 August 2010
Received in revised form 7 December 2010
Accepted 7 December 2010
Available online 14 December 2010

Keywords:
$Pt/Al_2O_3–CeO_2$
Nanocatalyst
Catalytic activity
VOC

ABSTRACT

$Pt/Al_2O_3–CeO_2$ nanocatalysts with Pt loading of 1% and ceria loading of 10, 20 and 30% were successfully prepared via wet impregnation method to be utilized in catalytic oxidation of BTX. The nanocatalysts were characterized using XRD, FESEM, TEM, N_2 adsorption, FTIR and TPR-H_2 techniques. The XRD patterns confirmed the formation of cerium oxide as the crystalline phase on alumina with the average crystallite size of 8.1–8.7 nm, derived by Scherrer equation. FESEM images confirmed that these nanocatalysts had ceria particles in nano-ranges. TEM analysis showed that platinum particles were fairly well dispersed on $Al_2O_3–CeO_2$ with an average size of 5–20 nm. BET surface area presented large surface area for nanocatalysts. TPR patterns showed that by adding 1% platinum to support, the reducibility is highly increased. These patterns also revealed the promoting effect of ceria on reducibility of Pt and Al_2O_3. The results of toluene oxidation indicated that the synthesized nanocatalysts were highly active and able to remove nearly 100% of toluene and xylene and about 85% of benzene as representative VOCs. The presence of nanoparticles along with good characteristics of the synthesized nanocatalysts presented them as highly efficient materials for catalytic oxidation of VOCs.

1. Introduction

Environmental issues especially air pollution is a global concern that requires efficient and economic methods for reducing pollutants like volatile organic compounds (VOCs). Among the various methods that can be used to control the emission of VOCs, catalytic oxidation is a very efficient and cost effective technology. This method can lower the temperature of the oxidation compared to thermal method and thus the lower energy is consumed and also the lower NO_x is emitted [1]. This aspect is due to usage of highly efficient catalysts. The catalysts which are used in oxidation of VOCs can be divided into three groups: supported noble metals, metal oxides or supported metals and mixtures of noble metals and metal oxides [1–6]. The selection of catalyst depends on some factors such as nature of the pollutants. Noble metals are known to be more active than metal oxides but the latter are more resistant to poisons and they are less expensive [7–10]. There are several factors that influence catalyst activity like active phase, loading, surface area of the catalyst, the dispersion of active compound and promoters [5]. There are some important factors that affect VOC degradation in catalytic oxidation reactions. The volatile organic compound structure is one important feature. O'Malley and Hodnett [11] showed that the reactivity of VOCs with different functional groups for total oxidation varies as alcohols > aromatics > ketones > carboxylic acids > alkanes [11]. Concentration is another important aspect. The effect of pollutant concentration on the conversion depends on type of incinerated VOC [12]. In oxidation of toluene and benzene, the conversion decreases as the concentration is increased [12]. Space velocity is also prominent. Increasing the space velocity, results in decreasing the conversion of VOCs [12]. The other important parameter is temperature. The higher the temperature, the more abatement is obtained.

The type of catalyst is also very important. For example, when comparing palladium and platinum, Pd is more active for the oxidation of short-chain hydrocarbons, while Pt exhibits higher activity toward long-chain hydrocarbons and aromatics [5].

C–H bond in saturated hydrocarbons is a crucial step in the combustion of these compounds. Once the first bond is broken, sequential reactions to CO_2 and H_2O are more facile. For example methane is the most difficult hydrocarbon to activate due to the strong C–H band that requires active catalyst as well as high temperatures. For longer C–C chains the activation of hydrocarbons becomes easier [1]. Promoters, active components, surface areas of

* Corresponding author at: Chemical Engineering Department, Sahand University of Technology, P.O. Box 51335-1996, Sahand New Town, Tabriz, Iran.
Tel.: +98 412 3458097/3459152; fax: +98 412 3444355.
E-mail address: haghighi@sut.ac.ir (M. Haghighi).
URL: http://rcrc.sut.ac.ir (M. Haghighi).

0304-3894/$ – see front matter © 2010 Elsevier B.V. All rights reserved.
doi:10.1016/j.jhazmat.2010.12.034

the catalysts, the extent of reducibility of the catalysts, and catalyst loading are other crucial factors affecting VOCs destruction [5]. The smaller the particle size, the better the catalyst activity [13].

Supported noble metals especially platinum on γ-Al_2O_3 catalysts have been used widely and efficiently for the oxidation of VOCs [14]. Although Pt is highly active in catalytic oxidation purposes, it is easily sintered and poisoned at relatively low temperatures and in this case catalyst deactivation occurs [14]. Ceria can play the role of promoter and reducible support. Its unique property of storing and releasing oxygen (redox property) makes it an attractive component for mixed oxide catalysts, since it can provide lattice oxygen and prevent the sintering of noble metals [15]. The redox property of ceria leads to oxygen vacancies resulting in high oxygen storage capacity. This feature helps the thermal resistance of the supports, the dispersion of supported metals, the oxidation and reduction of supported noble metals and the decrease in coke formation on the catalyst surface [16–22]. Ceria has the excellent thermal and mechanical resistance [23] and increases thermal stability of the support [22].

Ceria tends to be a nonstoichiometric compound with +4 and +3 oxidation states of cerium atom. Ceria has the unique redox property and the reduction of Ce^{4+} to Ce^{3+} as shown below leads to oxygen defects that makes ceria active enough for catalytic applications [24–29].

$$CeO_2 \underset{\text{Oxidizing}}{\overset{\text{Reducing}}{\rightleftarrows}} CeO_{2-y} + \frac{y}{2}O_2 \quad (0 \le y \le 0.5)$$

As particle size decreases, the concentration of Ce^{3+} relative to Ce^{4+} increases and hence more oxygen vacancies (defects) and more active sites are produced [24].

It is worth noting that the redox property of ceria would be enhanced by the presence of noble metal [30]. Also, it should be emphasized that ceria promotes the reduction of noble metals [22,31]. Therefore, in Pt/Al_2O_3–CeO_2 nanocatalyst, Pt and ceria have mutual interaction that promotes catalyst activity and stability. Cerium oxide is an effective promoter that in combination with mostly Pt and Al_2O_3 and other metal oxides has been used in many catalytic applications such as steam reforming reactions [32,33], wet air oxidations [34–36], partial oxidation of methane [31,37,38], water–gas shift reaction [39–41] as well as catalytic oxidation of VOCs [9,42–44]. Masui et al. used Pt/CeO_2–ZrO_2–Bi_2O_3/γ-Al_2O_3 catalysts for total oxidation of toluene [45]. The Pt/Al_2O_3–CeO_2 catalysts have been used for CO oxidation [46] and partial oxidation of methane [31]. However, to our knowledge using Pt/Al_2O_3–CeO_2 catalysts with nano characteristics for catalytic oxidation of BTX has not been reported in literature, so there was an enthusiasm to investigate this nano structured system for total oxidation of BTX.

Ceria is not as expensive as platinum but it is still expensive compared to γ-Al_2O_3 support. Therefore, by deposition of small amount of ceria over alumina a fairly cost effective catalyst can be achieved. Also, it does not have surface area as large as γ-Al_2O_3 and by deposition of ceria on a high surface area support like alumina, a carrier with high surface area and good redox property is achieved [47]. Therefore, by using a mixed oxide catalyst containing Pt, ceria and alumina, we can combine the benefits of high activity, high redox property and high surface area to reach a relatively inexpensive and highly effective catalyst for the oxidation of aromatic hydrocarbons. The aim of this work was to develop an efficient nanocatalyst with Pt as the active component, cerium oxide as an effective promoter and alumina as an inexpensive high surface area support to be utilized for VOC catalytic oxidation and air pollution reduction. Above all, the nanosized particles of Pt and CeO_2 on this nanostructured catalyst play a very important role in catalytic oxidation reaction. Reducing the particle size to nanoscale will provide a large number of more reactive sites [13]. In this research, Pt/Al_2O_3–CeO_2 nanocatalysts with 1% of platinum and different loadings of ceria over alumina were prepared. The synthesized catalysts were characterized by XRD, FESEM, TEM, BET, FTIR, and TPR-H_2. The activity of the catalysts was tested within the reaction conditions and the catalyst with the best activity was tested with different concentrations and weight hourly space velocity (WHSVs).

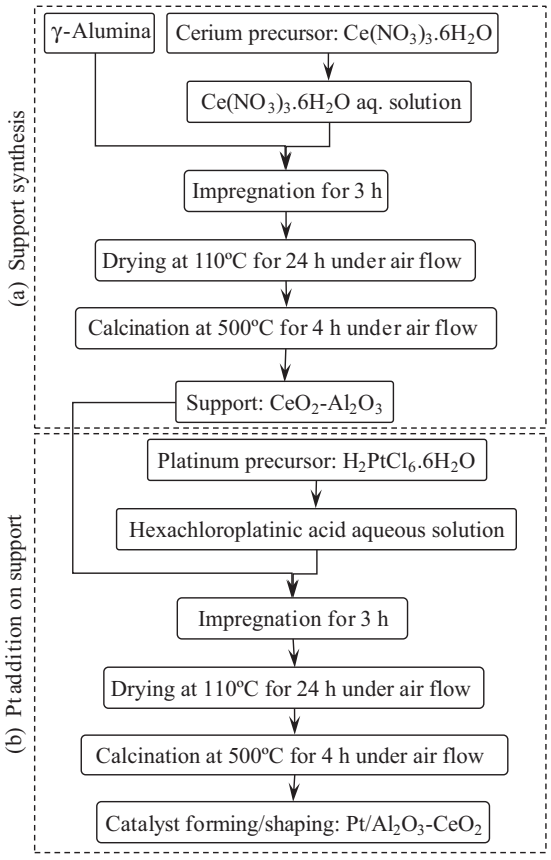

Fig. 1. Schematic flow chart for the preparation steps of Pt/Al_2O_3–CeO_2 nanocatalyst: (a) support synthesis and (b) addition of Pt on support.

2. Materials and methods

2.1. Materials

Hexachloroplatinic acid ($H_2PtCl_6{\cdot}6H_2O$) was used as Pt precursor. Cerium nitrate hexahydrate ($Ce(NO_3)_3{\cdot}6H_2O$) and γ-alumina were used as cerium precursor and support respectively. Toluene, xylene and benzene were used as representative VOCs for the investigation of catalysts activity. The materials were from Merck Company and were not purified further.

2.2. Catalyst synthesis and forming

Schematic flowchart for the preparation steps of nanostructured Pt/Al_2O_3–CeO_2 catalysts is illustrated in Fig. 1. The nanocatalysts were prepared via wet impregnation method. At first, a solution of cerium nitrate hexahydrate was prepared considering the appropriate loading of ceria on alumina. For example, for CeO_2(10%)/Al_2O_3, 2.8 g $Ce(NO_3)_3{\cdot}6H_2O$ was dissolved in 100 mL distilled water. Then the alumina support (10 g) was added to the solution and mixed for about 3 h. Next the mixture was dried at 110 °C for 24 h and calcined at 500 °C for 4 h under air flow. To this stage the Al_2O_3–CeO_2 support was prepared. In the next stage Pt was deposited on the synthesized support via wet impregna-

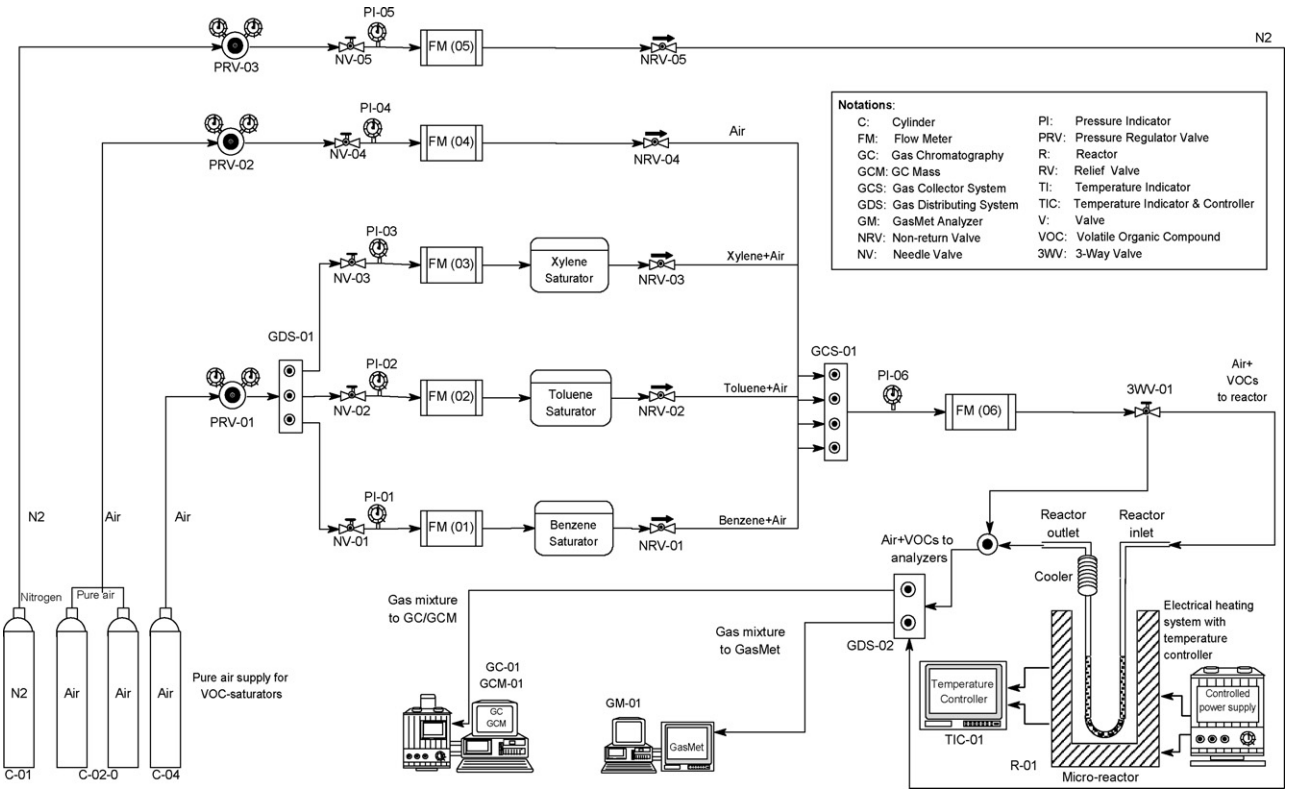

Fig. 2. Experimental setup for testing catalytic performance of synthesized nanocatalysts for toluene oxidation used for VOC abatement.

tion method to obtain $Pt/Al_2O_3–CeO_2$ with platinum loading of 1%. Thus a solution of hexachloroplatinic acid (0.266 g in 100 mL distilled water) was prepared and $Al_2O_3–CeO_2$ support was added to this solution. The mixture was mixed for 3 h and dried at 110 °C for 24 h. Then calcination was carried out at 500 °C for 4 h under air flow. The obtained powder was formed into cylindrical spices with 3 mm in diameter and 2 mm in height.

It should be mentioned that pure nano ceria was synthesized via redox reaction method. A solution of 0.5 M $Ce(NO_3)_3{\cdot}6H_2O$ was mixed with 30% hydrogen peroxide at a volume ratio of 3:1. Then the mixture was heated to reach boiling point. It was maintained at boiling temperature for 4 h. The remaining solution was then dried in oven at 110 °C for 24 h. Next, the solid was calcined at 500 °C for 4 h in air to get CeO_2 catalyst powder. The obtained powder was formed into cylindrical spices with 3 mm in diameter and 2 mm in height.

2.3. Catalyst characterization

The structure of catalysts was assessed using XRD analyzer (Bruker model D8 advance, Germany). Conditions of analysis were as follows: Cu-Kα radiation (λ = 1.54178 Å); scanning rate: 0.03°/s; scanning range (2θ): 20–80°.

The morphology and particle size of the nanostructure catalysts were observed by Field Emission Scanning Electron Microscopy (FESEM) analyzer (HITACHI S-4160). For detecting Pt particles on $Al_2O_3–CeO_2$, transmission electron microscopy (TEM) was carried out on a Philips CM-200. Samples for TEM measurements were ultrasonically dispersed in ethanol. Drops of suspensions were deposited on a copper grid coated with carbon.

The BET surface area of the catalysts was measured by N_2 adsorption at liquid-nitrogen temperature, using a surface area analyzer (Quantachrome chembet-3000).

For addressing surface functional groups, Fourier Transform Infrared Spectroscopy (FTIR, UNICAM 4600) was carried out in the range of 400–4000 cm^{-1} wave number.

TPR-H_2 measurements were carried out on a Micromeritics pulse chemisorb 2705 to address the reducibility of nanocatalysts. About 100 mg of the sample was loaded in a quartz reactor and pretreated at 150 °C in a He stream for 1 h to remove the adsorbed carbonates and hydrates. After cooling to room temperature, a flow of 10% H_2/Ar with 30 mL/min was passing through the samples and the temperature was raised at a rate of 10 °C/min up to 1000 °C while the TCD signal was recorded.

2.4. Catalyst performance test

Fig. 2 shows the utilized experimental setup for activity measurement of the synthesized nanocatalysts. Catalytic oxidation runs for abatement of BTX were performed in a U-shape Pyrex micro reactor (6 mm i.d.) at atmospheric pressure. For producing the gas stream containing toluene, xylene and benzene three saturators were utilized. Each saturator container has an inlet pathway for carrier gas (air). Air enters each saturator and diffuses through the liquid toluene, xylene or benzene. Then it carries some of these pollutants as vapour and exits from outlet pathway. For controlling the temperature of every saturator a mixture of ice and water was used. To obtain a precise concentration of pollutant, the flow rate of reactant passing through the saturator and the temperature of the bath containing ice and water should be controlled. The other air flow was mixed with polluted stream to stabilize the concentration of BTX containing stream. In order to precise control of flow rates, flow meters with needle valves were utilized. The micro reactor (6 mm i.d.) has an air condenser to cool down the exhaust gas stream to analyzers. The micro reactor is placed in an electrical furnace which provides the required temperature for catalytic reaction. About 0.5 g of nanocatalysts was placed in the

reactor for each run. Catalysts were placed between Pyrex balls. The catalytic experiments were evaluated in the temperature range of 120–300 °C. The samples were pretreated before each run at 120 °C to prevent overestimation of VOC removal caused by adsorption, because at the beginning of the tests the temperature is low and VOC may be removed mostly by adsorption rather than oxidation. The concentrations of the inlet and outlet gas stream were analyzed by GC–MS (Thermofinnigan, Italy) and GasMet (Dx-4000, Finland) analyzers. For activity tests of catalysts (Figs. 9 and 12), the total flow rate was set at 70 mL/min, the concentration of pollutant was 1000 ppm and WHSV = 8400 mL/hg. For the test that assessed the effect of WHSV, it was 4200 and 8400 mL/hg and the concentration was 1000 ppm. For the test that assessed the effect of pollutant concentration, it was varied from 1000 to 3600 ppm and WHSV was 8400 mL/hg.

3. Results and discussion

3.1. Nanocatalysts characterization

3.1.1. Crystallographic analysis

The XRD patterns of the synthesized $Pt/Al_2O_3–CeO_2$ nanocatalysts are shown in Fig. 3. The patterns for synthesized samples with platinum loading of 1% over pure alumina, $Al_2O_3–CeO_2$(10%), $Al_2O_3–CeO_2$(20%), $Al_2O_3–CeO_2$(30%) and pure ceria are illustrated in Fig. 3a, b, c, d and e respectively. As shown in the figure the XRD analysis demonstrates the formation of CeO_2 as indicated by the diffraction peak at 2θ = 28.7, 33.2, 47.7, 56.6, 59.4, 69.8, 77.1 and 79.5 corresponding to the planes of CeO_2. The diffraction lines of the synthesized ceria are typical of the cubic crystal structure of fluorite type oxide (JCPDS 01-075-0076). By comparison of XRD patterns, it is observed that with increasing the cerium oxide loading to 10, 20 and 30% over alumina, the peaks related to cerium oxide appears and becomes sharper. It can be identified that XRD data confirms the formation of CeO_2 as the crystalline phase on Al_2O_3 with the average crystallite size of 8.1–8.7 nm, derived by Scherrer equation which is less than the average crystallite size of pure ceria (10.5 nm).

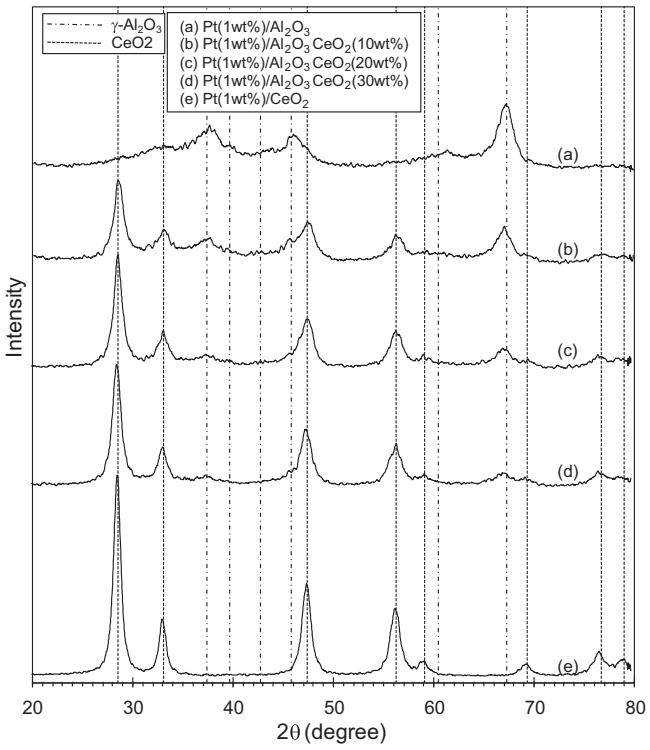

Fig. 3. XRD patterns of $Pt(1\ wt\%)/Al_2O_3–CeO_2$ nanocatalysts with different contents of ceria: (a) 0 wt% (pure Al_2O_3); (b) 10 wt%; (c) 20 wt%; (d) 30 wt%; (e) 100 wt% (pure CeO_2).

It should be noticed that in these patterns platinum oxide is not observed. This feature could be due to high dispersion of the Pt particles over the $Al_2O_3–CeO_2$ support which may be the result of well impregnation and calcination conditions (500 °C and 4 h).

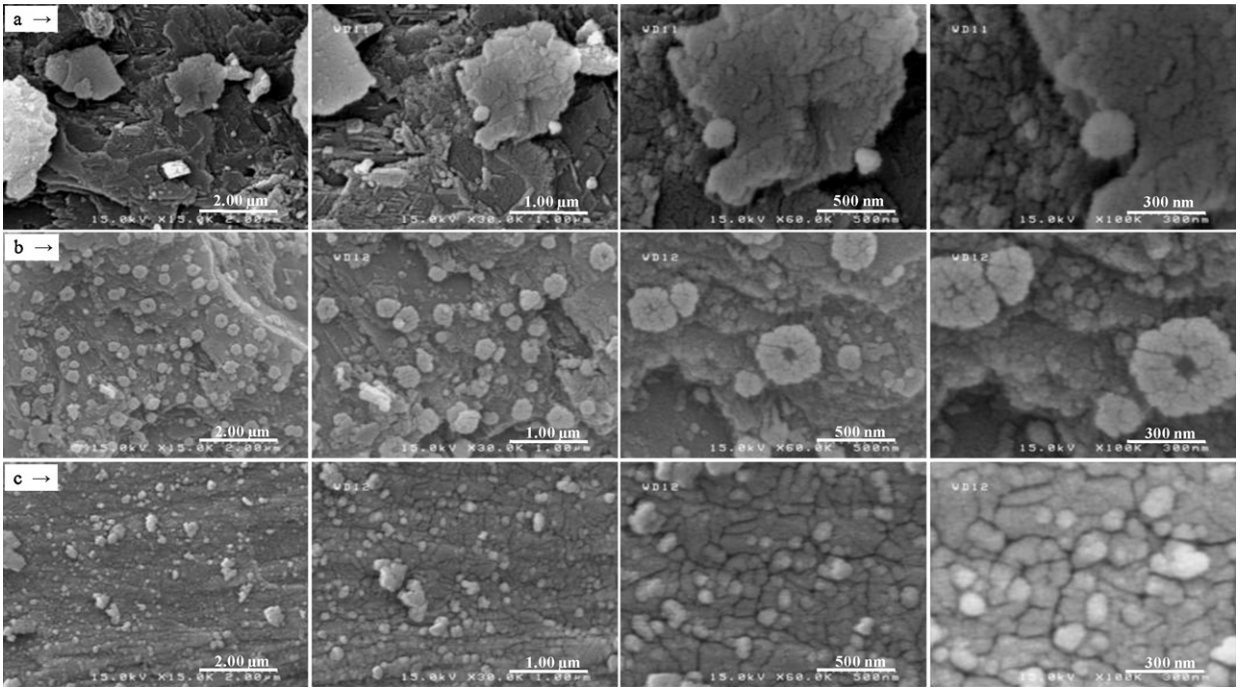

Fig. 4. FESEM images of $Pt(1\ wt\%)/Al_2O_3$ (a), $Pt(1\ wt\%)/Al_2O_3–CeO_2$(20 wt%) (b) and $Pt(1\ wt\%)/CeO_2$ (c).

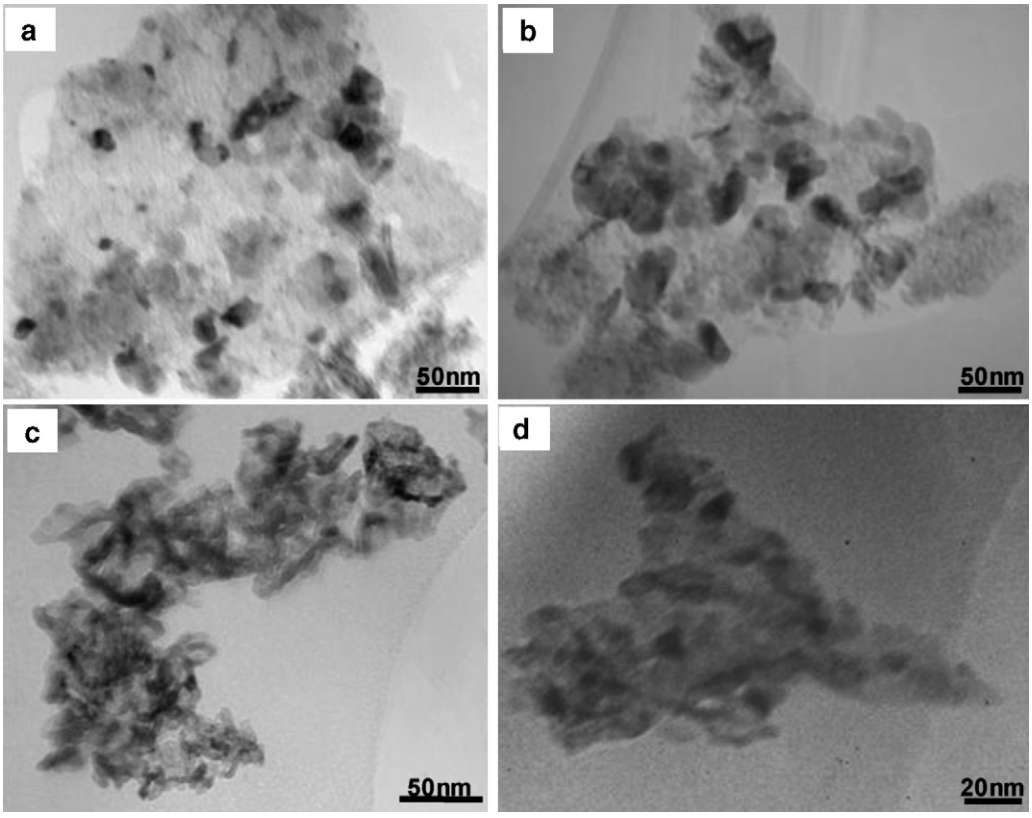

Fig. 5. TEM images of Pt(1 wt%)/CeO_2 (a and b) and Pt(1 wt%)/Al_2O_3–CeO_2(30 wt%) (c and d).

3.1.2. FESEM analysis

FESEM images of synthesized Pt(1%)/Al_2O_3, Pt(1%)/Al_2O_3–CeO_2(20%) and Pt(1%)/CeO_2 are shown in Fig. 4a, b and c respectively. In Fig. 4b, the particles of cerium oxide can be found among pieces of alumina support with particle size of around 10–50 nm. Comparison of Fig. 4b and c shows that nano ceria has been formed successfully on alumina support and has nanostructures almost as the same size of nano ceria in Fig. 4c. Nano particles provide more reactive and reducible sites and results to a high catalytic performance of the catalyst. Furthermore, this nanocatalyst has the advantage of precious metal and ceria promoter with the nano scale particles deposited on an inexpensive high surface area support that makes it a very suitable catalyst for VOC removal.

3.1.3. TEM analysis

The morphology and microstructure of synthesized catalysts were investigated by TEM techniques. Fig. 5 shows TEM images of Pt(1%)/CeO_2 (a and b) and Pt(1%)/Al_2O_3–CeO_2(30%) (c and d). It is shown that the active phase (Pt) is fairly well dispersed with a particle size of 5–20 nm. The presence of nano CeO_2 was shown by FESEM images (Fig. 4). The presence of Pt nanoparticles cannot be detected by FESEM images, so TEM analysis was used to determine Pt nanoparticles. Noble metal/CeO_2 systems promote the migration/exchange of the oxygen species [48]. Therefore, apart from the mutual interaction of Pt and ceria, their existence in form of nanoparticles helps to provide catalyst with much more reactive sites.

3.1.4. BET surface area

Fig. 6 shows the results of BET surface area of the synthesized samples. It is observed that nanostructured Pt/Al_2O_3–CeO_2 catalysts have high surface area for the oxidation of volatile organics. For Pt/Al_2O_3 it can be seen that the surface area is 107 m^2/g. Adding ceria content of 10, 20 and 30% leads to the decrease of the surface area to 92, 78 and 68 m^2/g respectively. Increasing the content of ceria leads to covering the surface of alumina and the overall surface area is decreased. The high surface area results in more adsorption sites for pollutants to be oxidized. Adsorption is one of the important steps of a catalytic reaction and the surface area of the catalyst is a very important need for adsorption of volatile organics. The high surface area could be a result of nanometric particles and suitable calcination temperature (500 °C).

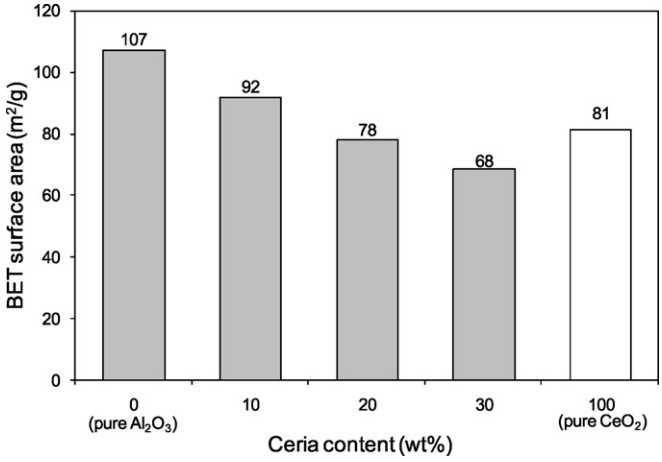

Fig. 6. BET surface area of Pt(1 wt%)/Al_2O_3–CeO_2 nanocatalysts with different contents of ceria.

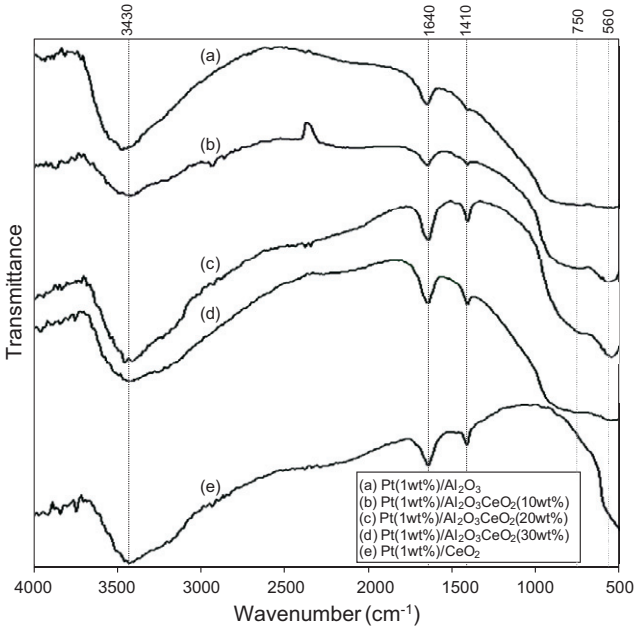

Fig. 7. FTIR spectrum of Pt(1 wt%)/Al_2O_3–CeO_2 nanocatalysts with different contents of ceria: (a) 0 wt% (pure Al_2O_3); (b) 10 wt%; (c) 20 wt%; (d) 30 wt%; (e) 100 wt% (pure CeO_2).

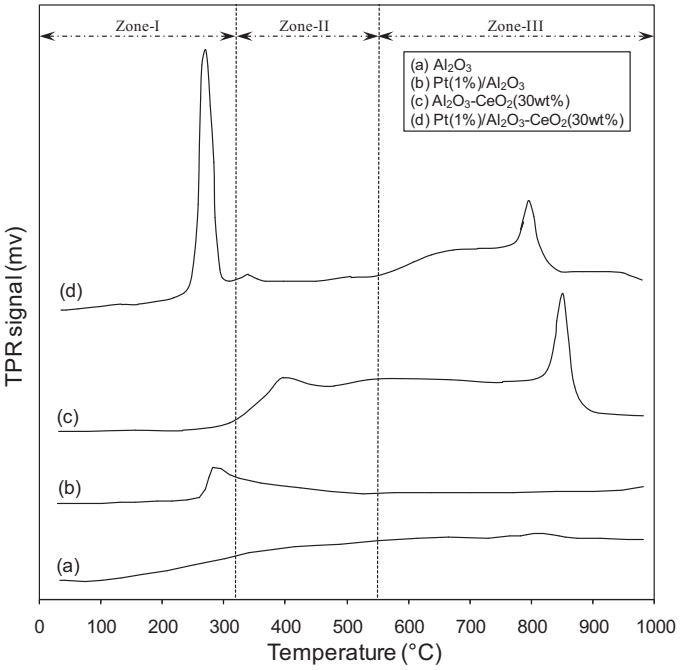

Fig. 8. TPR-H_2 profiles of synthesized Pt-catalysts: (a) Al_2O_3, (b) Pt(1%)/Al_2O_3, (c) Al_2O_3–CeO_2(30%) and (d) Pt(1%)/Al_2O_3–CeO_2(30%).

3.1.5. FTIR analysis

FTIR spectra of the samples are shown in Fig. 7. The stretching vibration for structural –OH and adsorbed water at wave number about 3430, 1640 and 1410 cm^{-1} for all samples were observed [49,50]. These vibrations imply to physically adsorbed water in all samples after catalysts heat treatment. However, the 1410 cm^{-1} peak is less intense for alumina without ceria and alumina containing 10% ceria. In samples (a), (b), (c) and (d) in the figure, existence of Al–O and CeO–O bonds and in sample (e) Ce–O bond was expected. Characteristic vibrational bands next to 570 cm^{-1} for Al–O [51] and around 700 cm^{-1} for Ce–O [52,53] have been reported. A band between 500 and 800 cm^{-1} for samples (a), (b), (c) and (d) was observed. This band may be attributed to the overlapped Ce–O and Al–O bonds. FTIR spectra recorded for sample (e) shows a significant change near 700 cm^{-1} which is attributed to Ce–O bonding and stretching around 500 cm^{-1} can be attributed to oxygen existence in sample.

3.1.6. TPR-H_2 analysis

The TPR-H_2 patterns of pure Al_2O_3, Pt(1%)/Al_2O_3, Al_2O_3–CeO_2(30%) and Pt(1%)/Al_2O_3–CeO_2(30%) are shown in Fig. 8a, b, c and d respectively. There is no hydrogen consumption on the TPR profile of Pure Al_2O_3. For Pt(1%)/Al_2O_3, there is a small reduction peak in Zones I and II at the temperature range of about 260–500 °C. This peak is centered at around 290 °C and could be assigned to Pt-oxide species and/or to reduction of $PtCl_xO_y$ (oxychloroplatinum surface complexes) species [17,31,38]. It can be seen from Fig. 8c that reduction bands shown belong to CeO_2 in zones II and III in the temperature range of 320–1000 °C. It can be seen from the figure that reduction bands shown in the Al_2O_3–CeO_2(30%) pattern belong to CeO_2 in Zones II and III in the range of 320–1000 °C. The peak at around 320–550 °C (Zone-II) would be assigned to the reduction of surface CeO_2. The second peak observed at around 800–1000 °C (Zone-III) could be attributed to the reduction of bulk CeO_2 to Ce_2O_3 [39,54]. It should be mentioned that reduction of ceria occurs first on the surface and then affects the bulk. The initial progress of reduction is highly sensitive to the surface area of the samples. Bulk reduction begins only when all surface sites are completely reduced. Hence, the peak in Zone-III can be attributed to the total reduction of ceria by elimination of O^{2-} anion of the lattice and formation of Ce_2O_3 [55].

In the TPR profile of Pt(1%)/Al_2O_3–CeO_2(30%) (Fig. 8d), the peak attributed to superficial reduction of CeO_2, is shifted to lower temperature (Fig. 8c). This feature proposes that the surface reduction of CeO_2 is enhanced by the presence of Pt. This suggests that the presence of Pt over ceria surface leads to easier reduction of the surface of CeO_2 influenced by the hydrogen spillover from the metallic platinum particles to cerium oxide. This peak is centered at around 270 °C and with a shoulder at 340 °C and corresponds to the reduction of $PtCl_xO_y$ (oxychloroplatinum complexes) species and to the reduction of superficial ceria promoted by platinum. In Pt(1%)/Al_2O_3–CeO_2(30%) profile, the second peak correlated to the reduction of bulk ceria (Zone-III) is moved to a less extent to lower temperature suggesting that the addition of Pt does not affect the bulk reduction of ceria as much as surface reduction of ceria. These observations are in good agreement with literature data [31,38]. The presence of ceria on alumina leads to a decrease in the temperature of reduction of platinum oxide species [17]. This aspect can be seen from Fig. 8d, since the reduction peak of Pt(1%)/Al_2O_3 (Zone-I), is moved to a low temperature and with much more area (Fig. 8d, Zone-I) suggesting that ceria can enhance the reduction of Pt-oxide species. This mutual interaction causes a better performance of the catalyst as it is confirmed by catalyst activity in Figs. 9–12. Reducibility of cerium oxide depends on the size of nanocrystallites. Smaller the size of the crystallites, higher the reducibility and furthermore the higher the activity [56]. The effect of Pt and ceria on the reductive properties of synthesized nanocatalyst is shown by the amount of hydrogen consumption (Table 1). By comparison of Al_2O_3–CeO_2(30%) and Pt(1%)/Al_2O_3–CeO_2(30%) hydrogen consumption, it is realized that the presence of platinum causes a better reduction and more hydrogen consumption of nanocatalysts. Also comparison of hydrogen consumption in Pt(1%)/Al_2O_3–CeO_2(30%) and Pt(1%)/Al_2O_3 indicates that the presence of ceria enhances the reduction of platinum particles. This mutual interaction leads to better reactivity of nanocatalyst for the oxidation of volatile organics.

Table 1
H_2 consumption in TPR-H_2 analysis of synthesized nanocatalysts.

Sample	Temperature (°C)	Hydrogen consumption (μmol H_2/g)
Al_2O_3–CeO_2(30%)		
Peak 1	400	15
Peak 2	850	115.05
Pt(1%)/Al_2O_3–CeO_2(30%)		
Peak 1	260	275.93
Peak 2	800	68.76
Pt(1%)/Al_2O_3		
Peak 1	295	45.52

3.2. Nanocatalysts performance studies for BTX oxidation

3.2.1. Nanocatalysts oxidation performance vs. temperature for abatement of toluene

Fig. 9 presents the catalytic activities for toluene oxidation as a function of reaction temperature. The conversion of toluene over nanocatalysts for Pt(1%)/Al_2O_3–CeO_2(30%) is around 100% at 250 °C while other nanocatalysts have lower activity at this temperature. It is identified from the figure that for synthesized nanocatalysts, the activity increases by raising the amount of ceria loading. However it can be seen from the figure that Pt(1%)/Al_2O_3 has more activity than Pt(1%)/Al_2O_3–CeO_2(10%) and less activity than Pt(1%)/Al_2O_3–CeO_2(20%) and Pt(1%)/Al_2O_3–CeO_2(30%) nanocatalysts suggesting that the promoting effect of higher loading of cerium oxide. It should be noticed that usage of noble metal along with reducible oxide has the advantage of combining high activity and stability [57].

The oxidation efficiency for Pt(1%)/CeO_2 nanocatalyst at around 200 °C is about 84% which is more than that of Pt(1%)/Al_2O_3–CeO_2(30%) nanocatalyst (78%), however, after this temperature the activity becomes lower than the activity of Pt(1%)/Al_2O_3–CeO_2(30%). This behavior can be addressed by better dispersion of ceria and platinum particles over alumina carrier in Pt(1%)/Al_2O_3–CeO_2(30%) compared to lower dispersion of Pt on cerium oxide in Pt(1%)/CeO_2. Another reason could be the smaller crystallite size of the Pt(1%)/Al_2O_3–CeO_2(30%) (8.2 nm) compared to the crystallite size of Pt(1%)/CeO_2 (10.5 nm). Complete destruction at 250 °C was only achieved for Pt(1%)/Al_2O_3–CeO_2(30%) so this nanostructured catalyst can be considered as the most suitable catalyst for catalytic oxidation of toluene. There is a deviation at temperature below 185 °C for alumina supported ceria catalysts that shows less activity for higher ceria loading (20 and 30%) in comparison to 10% of ceria. This aspect could be addressed by adsorption effect at the beginning of the experiments that resulted in more VOC elimination for Pt(1%)/Al_2O_3–CeO_2(10%) and Pt(1%)/Al_2O_3–CeO_2(20%) compared to Pt(1%)/Al_2O_3–CeO_2(30%).

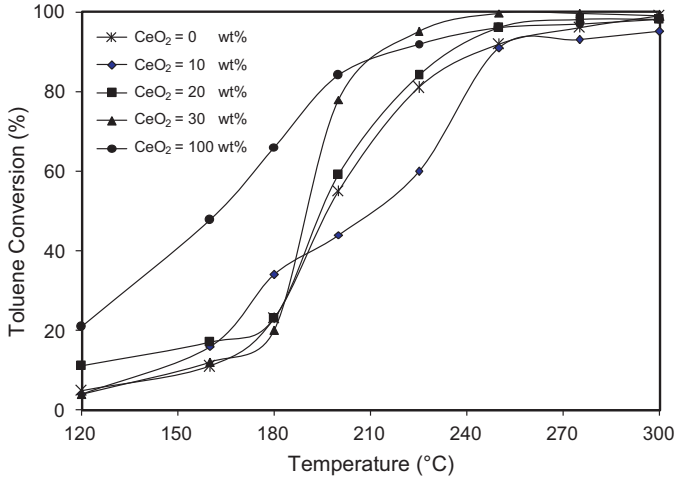

Fig. 9. The performance of Pt(1%)/Al_2O_3–CeO_2 nanocatalysts with different contents of ceria for toluene oxidation.

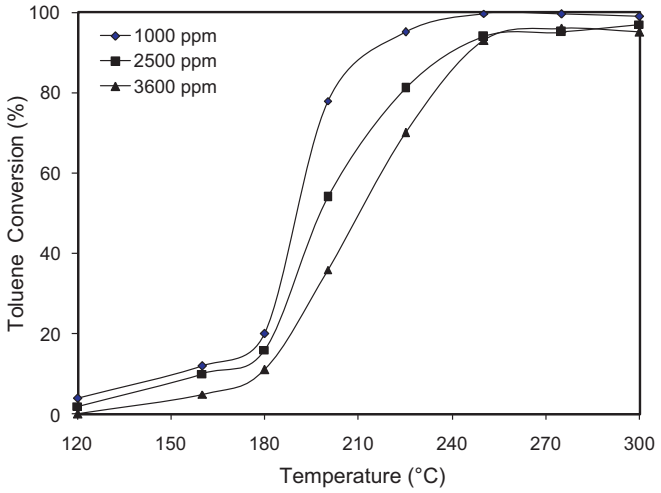

Fig. 10. Oxidation performance of synthesized Pt(1 wt%)/Al_2O_3–CeO_2(30 wt%) nanocatalyst at different toluene concentrations in polluted air for abatement of toluene.

3.2.2. Oxidation performance of synthesized nanocatalysts at different toluene concentrations

The effect of toluene concentration on the Pt(1%)/Al_2O_3–CeO_2(30%) in oxidation process is shown in Fig. 10. It is observed from the figure that increasing the concentration of toluene results in decreasing of the catalyst activity. As can be seen 100% removal of toluene could be achieved in the concentration of 1000 ppm at 250 °C while in 2500 ppm and 3600 ppm the conversion was about 95%. Even at higher concentrations of toluene (3600 ppm) the nanostructured catalyst has still enough destruction ability to reduce the pollutant.

3.2.3. Oxidation performance of synthesized nanocatalysts at different WHSVs for abatement of toluene

The performance of Pt(1%)/Al_2O_3–CeO_2(30%) nanocatalyst with different WHSVs was investigated and presented in Fig. 11. For both WHSVs complete removal efficiency was observed regarding the fact that removal percent for 4200 mL/hg and 8400 mL/hg at 225 °C

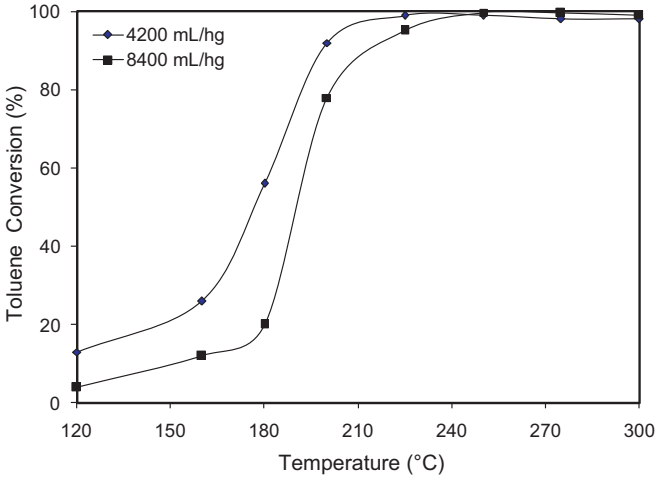

Fig. 11. Oxidation performance of synthesized Pt(1 wt%)/Al_2O_3–CeO_2(30 wt%) nanocatalyst at different WHSVs for abatement of toluene.

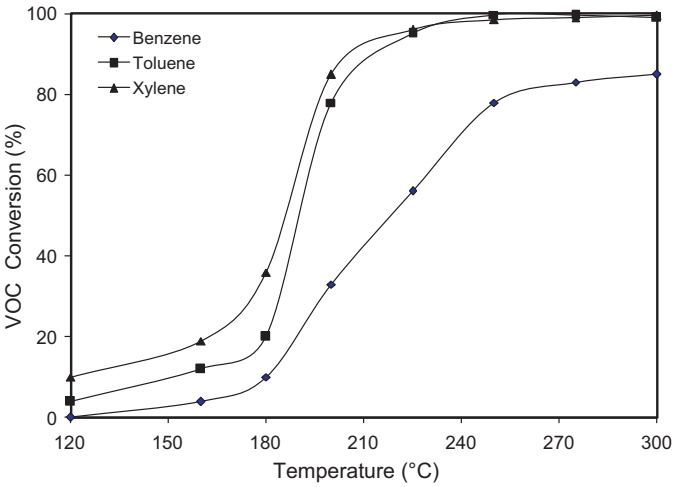

Fig. 12. Comparison of catalytic performance of synthesized Pt(1 wt%)/Al_2O_3–CeO_2(30 wt%) nanocatalyst for total oxidation of benzene, toluene and xylene.

was 99 and 95% respectively. It is shown that, even by doubling the weigh hourly space velocity, a very good activity toward catalytic oxidation of toluene as representative VOC is achieved.

3.2.4. Oxidation performance of synthesized nanocatalysts for abatement of different VOCs

The ability of the synthesized nanocatalyst was investigated using BTX and presented in Fig. 12. Catalytic oxidation is influenced greatly by the nature of the pollutants. Regarding the fact that binding energy is different in various volatile organics, different activities and removal efficiencies are expected for different pollutants at the same reaction condition. It is realized from the figure that the complete destruction (about 100%) of xylene and toluene was achieved at 250 °C while the removal percent of benzene at this temperature was approximately 78%. This observation could be assigned to the different adsorption behaviors and activation energies of the pollutants. Xylene has two methyl groups and toluene has one methyl group and they are better adsorbed on the support and consequently better oxidation and removal destruction is achieved while benzene is a completely stable compound and without any methyl group. Toluene is more distorted than benzene and since the aromatic ring is an electron donor, the stability of the π-complex is increased by the presence of the methyl group. Flat adsorption and formation of a π-complex have also been demonstrated for o- and p-xylene. Toluene and xylene are less stable than benzene on the surface. The complex stability (and therefore the strength of the adsorption bond) is determined by the ionization potential of the donor molecule: the alkyl groups increase the electron density in the benzene ring, so the ionization potential is decreased and the formation of a charge transfer complex is promoted. The ionization potential decreases in the order of benzene > toluene > p-xylene. So it can be concluded that since toluene and xylene have lower ionization potential than benzene, they are better adsorbed on the surface [58]. Another reason that could be mentioned here is that the adsorption of molecules depend on the molecular weight, so toluene and xylene have molecular weight greater than benzene and they are better adsorbed on the surface.

Therefore, due to less adsorption, more binding energy of carbon atoms and more stability of aromatic ring, benzene is more difficult to be oxidized than xylene and toluene. Despite this difficulty toward oxidation of benzene, 85% removal of this pollutant is obtained at 300 °C.

3.3. Reaction mechanism

The mechanism of complete catalytic oxidation depends on the type of catalyst which is used.

Noble metals may follow either a Longmuir–Hinshelwood type of mechanism (reaction between adsorbed oxygen and an adsorbed reactant) or an Elay–Rideal mechanism (reaction between adsorbed oxygen and a gas-phase reactant molecule) [59].

The general mechanism of oxidation over noble metals is considered to involve the dissociative adsorption of oxygen:

$$O_2 + [\,] \xrightarrow{\text{fast}} 2[O]$$

where [ ] represents an available "surface site". This step is then followed by direct reaction of the gaseous organic reactant with [O].

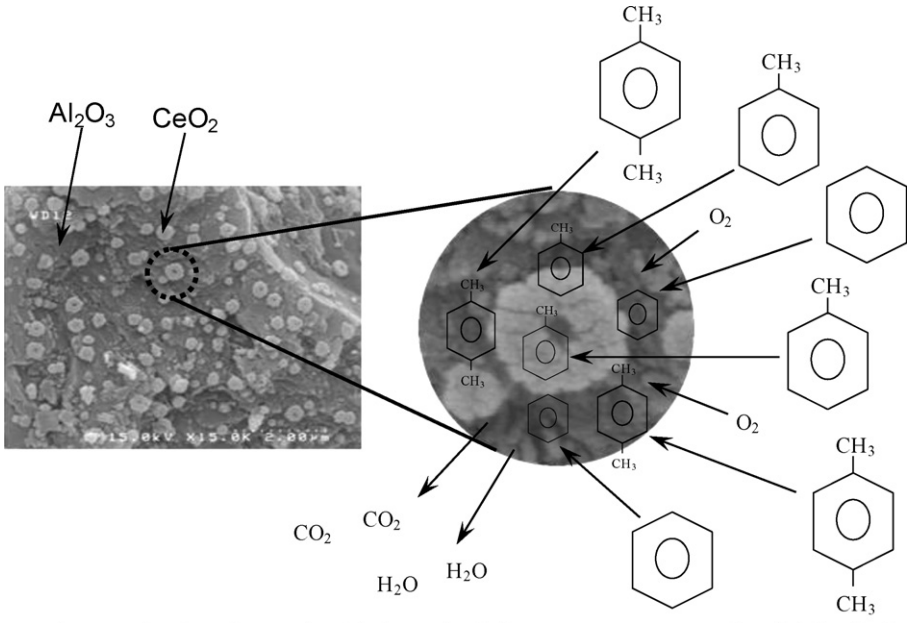

Fig. 13. Reaction mechanism for total oxidation of VOCs over nanostructured Pt/Al_2O_3–CeO_2 catalysts.

However, sometimes the reactant can be weakly adsorbed first. It has been proposed that oxidation often occurs by a parallel-series mechanism according to the following reaction schematic:

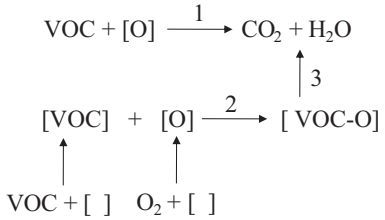

In cerium oxide the reaction mechanism is the conventional redox or Mars–van Krevelen cycle, which involves the oxidation and reduction of the metal oxide. The Mars–van Krevelen mechanism of catalytic oxidations over metal oxides is a redox mechanism involving both gas phase and lattice oxygen.

$$MeO + VOC \rightarrow VOC - O + Me$$

$$2Me + O_2 \rightarrow 2MeO$$

where Me is a metal cation and VOC is a hydrocarbon reactant. The mechanism of catalytic oxidation on mixed metal oxides is thought to be similar at least in principle to that on single metal oxides. The activity of mixed oxides is generally higher than single oxide components. Lattice oxygen, as well as gas-phase oxygen, participates in the catalytic oxidation process. The process is a redox cycle at the oxide surface with anionic oxygen from the surface (either chemisorbed or lattice oxygen) reacting with a chemisorbed or gas-phase organic reactant [59].

Toluene is assumed to be oxidized on both Pt and CeO_2. The presence of Pt in the catalyst enhances the redox behavior of CeO_2. On Pt, toluene reacts with O_2 from gas phase which is weakly adsorbed on Pt. However, on CeO_2 toluene can react with the both weakly adsorbed O_2 and lattice oxygen. Therefore the reaction mechanism for oxidation on Pt could be Elay–Rideal or Longmuir–Hinshelwood, but mechanism for oxidation on CeO_2 is Mars–van Krevelen.

Balcaen et al. have shown a schematic representation of the steps in the oxidation of propane over $CuO–CeO_2/Al_2O_3$ catalyst [60]. A similar representation of the steps in complete oxidation of toluene over $Pt/Al_2O_3–CeO_2$ has been provided here to demonstrate the oxidation mechanism on the prepared nanostructured catalysts in this work in Fig. 13.

4. Conclusions

$Pt(1\%)/Al_2O_3–CeO_2(30\%)$ nanostructure catalysts were successfully synthesized using wet impregnation method. The XRD analysis revealed that nano cerium oxide was formed as the crystalline phase on alumina with the average crystallite size of 8.1–8.7 nm, derived by Scherrer equation. Morphological analysis indicated that the synthesized nanocatalysts had nanoparticles (ceria and Pt) in nano-ranges. BET surface area measurements showed that the nanocatalysts had large surface area for catalytic application. TPR analysis addressed that Pt over alumina supported ceria was highly reducible due to the presence of platinum as the active compound and ceria as the promoter. These patterns also revealed the promoting effect of ceria on reducibility of Pt and Al_2O_3. The activity experiments revealed that among synthesized nanocatalysts, $Pt(1\%)/Al_2O_3–CeO_2(30\%)$ and $Pt(1\%)/CeO_2$ had the highest activity for abatement of toluene with the superior activity of $Pt(1\%)/Al_2O_3–CeO_2(30\%)$. The $Pt(1\%)/Al_2O_3–CeO_2(30\%)$ nanocatalyst was chosen as an inexpensive effective catalyst since it benefits from ceria promoter and Pt to provide an efficient catalyst capable of complete destruction of toluene at 250 °C and high removal efficiency of BTX at different concentrations and WHSVs.

Acknowledgements

The authors gratefully acknowledge Sahand University of Technology for the financial support of the project as well as Tabriz Refinery Company and Iran Nanotechnology Initiative Council for complementary financial support. They also wish to thank Institute of Polymeric Materials for providing the facilities for catalyst forming and Mr. Jafarizad for the technical aid at analytical lab of chemical engineering department.

References

[1] A.C. Gluhoi, B.E. Nieuwenhuys, Catalytic oxidation of saturated hydrocarbons on multicomponent Au/Al_2O_3 catalysts: effect of various promoters, Catalysis Today 119 (2007) 305–310.
[2] S.C. Kim, The catalytic oxidation of aromatic hydrocarbons over supported metal oxide, Journal of Hazardous Materials 91 (2002) 285–299.
[3] Y. Li, X. Zhang, H. He, Y. Yu, T. Yuan, Z. Tian, J. Wang, Y. Li, Effect of the pressure on the catalytic oxidation of volatile organic compounds over Ag/Al_2O_3 catalyst, Applied Catalysis B: Environmental 89 (2009) 659–664.
[4] J. Chi-Sheng Wu, T.-Y. Chang, VOC deep oxidation over Pt catalysts using hydrophobic supports, Catalysis Today 44 (1998) 111–118.
[5] S. Ojala, Catalytic Oxidation of Volatile Organic Compounds and Malodorous Organic Compounds, University of Oulu, 2005.
[6] P. Papaefthimiou, T. Ioannides, X.E. Verykios, Combustion of non-halogenated volatile organic compounds over group VIII metal catalysts, Applied Catalysis B: Environmental 13 (1997) 175–184.
[7] F. Bertinchamps, Total Oxidation of Chlorinated VOCs on Supported Oxide Catalysts, UCL – AGRO/CABI – Département de chimie appliquée et des bio-industries, Université catholique de Louvain, 2005.
[8] C.T. Wong, A.Z. Abdullah, S. Bhatia, Catalytic oxidation of butyl acetate over silver-loaded zeolites, Journal of Hazardous Materials 157 (2008) 480–489.
[9] C.-H. Wang, S.-S. Lin, Preparing an active cerium oxide catalyst for the catalytic incineration of aromatic hydrocarbons, Applied Catalysis A: General 268 (2004) 227–233.
[10] D. Delimaris, T. Ioannides, VOC oxidation over $CuO–CeO_2$ catalysts prepared by a combustion method, Applied Catalysis B: Environmental 89 (2009) 295–302.
[11] A. O'Malley, B.K. Hodnett, The influence of volatile organic compound structure on conditions required for total oxidation, Catalysis Today 54 (1999) 31–38.
[12] J. Hermia, S. Vigneron, Catalytic incineration for odour abatement and VOC destruction, Catalysis Today 17 (1993) 349–358.
[13] W. Shen, X. Dong, Y. Zhu, H. Chen, J. Shi, Mesoporous CeO_2 and CuO-loaded mesoporous CeO_2: synthesis, characterization, and CO catalytic oxidation property, Microporous and Mesoporous Materials 85 (2005) 157–162.
[14] H.S. Kim, T.W. Kim, H.L. Koh, S.H. Lee, B.R. Min, Complete benzene oxidation over Pt–Pd bimetal catalyst supported on [gamma]-alumina: influence of Pt–Pd ratio on the catalytic activity, Applied Catalysis A: General 280 (2005) 125–131.
[15] H. Liu, L. Ma, S. Shao, Z. Li, A. Wang, Y. Huang, T. Zhang, Preferential CO oxidation on Ce-promoted Pt/[gamma]-Al_2O_3 catalysts under H_2-rich atmosphere, Chinese Journal of Catalysis 28 (2007) 1077–1082.
[16] A. Parinyaswan, S. Pongstabodee, A. Luengnaruemitchai, Catalytic performances of $Pt–Pd/CeO_2$ catalysts for selective CO oxidation, International Journal of Hydrogen Energy 31 (2006) 1942–1949.
[17] S. Damyanova, J.M.C. Bueno, Effect of CeO_2 loading on the surface and catalytic behaviors of $CeO_2–Al_2O_3$-supported Pt catalysts, Applied Catalysis A: General 253 (2003) 135–150.
[18] P. Djinovic, J. Levec, A. Pintar, Effect of structural and acidity/basicity changes of $CuO–CeO_2$ catalysts on their activity for water–gas shift reaction, Catalysis Today 138 (2008) 222–227.
[19] X.-S. Huang, H. Sun, L.-C. Wang, Y.-M. Liu, K.-N. Fan, Y. Cao, Morphology effects of nanoscale ceria on the activity of Au/CeO_2 catalysts for low-temperature CO oxidation, Applied Catalysis B: Environmental 90 (2009) 224–232.
[20] D. Andreeva, R. Nedyalkova, L. Ilieva, M.V. Abrashev, Nanosize gold-ceria catalysts promoted by vanadia for complete benzene oxidation, Applied Catalysis A: General 246 (2003) 29–38.
[21] S. Bernal, G. Blanco, J.M. Pintado, J.M. Rodríguez-Izquierdo, M.P. Yeste, An alternative way of reporting on the redox behaviour of ceria-based catalytic materials: temperature-chemical environment-oxidation state diagrams, Catalysis Communications 6 (2005) 582–585.
[22] R. Ramírez-López, I. Elizalde-Martinez, L. Balderas-Tapia, Complete catalytic oxidation of methane over $Pd/CeO_2–Al_2O_3$: the influence of different ceria loading, Catalysis Today 150 (2010) 358–362.
[23] L.S.F. Feio, C.E. Hori, S. Damyanova, F.B. Noronha, W.H. Cassinelli, C.M.P. Marques, J.M.C. Bueno, The effect of ceria content on the properties of $Pd/CeO_2/Al_2O_3$ catalysts for steam reforming of methane, Applied Catalysis A: General 316 (2007) 107–116.
[24] D. Schubert, R. Dargusch, J. Raitano, S.-W. Chan, Cerium and yttrium oxide nanoparticles are neuroprotective, Biochemical and Biophysical Research Communications 342 (2006) 86–91.
[25] Y. Wei, H. Wang, F. He, X. Ao, C. Zhang, CeO_2 as the oxygen carrier for partial oxidation of methane to synthesis gas in molten salts: thermodynamic analysis

and experimental investigation, Journal of Natural Gas Chemistry 16 (2007) 6–11.
[26] M.A. Centeno, M. Paulis, M. Montes, J.A. Odriozola, Catalytic combustion of volatile organic compounds on $Au/CeO_2/Al_2O_3$ and Au/Al_2O_3 catalysts, Applied Catalysis A: General 234 (2002) 65–78.
[27] D. Andreeva, R. Nedyalkova, L. Ilieva, M.V. Abrashev, Gold-vanadia catalysts supported on ceria-alumina for complete benzene oxidation, Applied Catalysis B: Environmental 52 (2004) 157–165.
[28] Q. Dai, X. Wang, G. Lu, Low-temperature catalytic combustion of trichloroethylene over cerium oxide and catalyst deactivation, Applied Catalysis B: Environmental 81 (2008) 192–202.
[29] M. Kang, M.W. Song, C.H. Lee, Catalytic carbon monoxide oxidation over CoO_x/CeO_2 composite catalysts, Applied Catalysis A: General 251 (2003) 143–156.
[30] L. Pino, A. Vita, M. Cordaro, V. Recupero, M.S. Hegde, A comparative study of Pt/CeO_2 catalysts for catalytic partial oxidation of methane to syngas for application in fuel cell electric vehicles, Applied Catalysis A: General 243 (2003) 135–146.
[31] A.C.S.F. Santos, S. Damyanova, G.N.R. Teixeira, L.V. Mattos, F.B. Noronha, F.B. Passos, J.M.C. Bueno, The effect of ceria content on the performance of $Pt/CeO_2/Al_2O_3$ catalysts in the partial oxidation of methane, Applied Catalysis A: General 290 (2005) 123–132.
[32] P. Ciambelli, V. Palma, A. Ruggiero, Low temperature catalytic steam reforming of ethanol. 2. Preliminary kinetic investigation of Pt/CeO_2 catalysts, Applied Catalysis B: Environmental 96 (2010) 190–197.
[33] W.L.S. Faria, C.A.C. Perez, D.V. César, L.C. Dieguez, M. Schmal, In situ characterizations of Pd/Al_2O_3 and $Pd/CeO_2/Al_2O_3$ catalysts for oxidative steam reforming of propane, Applied Catalysis B: Environmental 92 (2009) 217–224.
[34] P. Massa, F. Ivorra, P. Haure, F.M. Cabello, R. Fenoglio, Catalytic wet air oxidation of phenol aqueous solutions by 1% $Ru/CeO_2–Al_2O_3$ catalysts prepared by different methods, Catalysis Communications 8 (2007) 424–428.
[35] C. Milone, M. Fazio, A. Pistone, S. Galvagno, Catalytic wet air oxidation of p-coumaric acid on CeO_2, platinum and gold supported on CeO_2 catalysts, Applied Catalysis B: Environmental 68 (2006) 28–37.
[36] L. Chang, I.P. Chen, S.-S. Lin, An assessment of the suitable operating conditions for the CeO_2/[gamma]-Al_2O_3 catalyzed wet air oxidation of phenol, Chemosphere 58 (2005) 485–492.
[37] H. Tanaka, R. Kaino, K. Okumura, T. Kizuka, K. Tomishige, Catalytic performance and characterization of $Rh-CeO_2/MgO$ catalysts for the catalytic partial oxidation of methane at short contact time, Journal of Catalysis 268 (2009) 1–8.
[38] F.A. Silva, D.S. Martinez, J.A.C. Ruiz, L.V. Mattos, C.E. Hori, F.B. Noronha, The effect of the use of cerium-doped alumina on the performance of $Pt/CeO_2/Al_2O_3$ and $Pt/CeZrO_2/Al_2O_3$ catalysts on the partial oxidation of methane, Applied Catalysis A: General 335 (2008) 145–152.
[39] Q. Yu, W. Chen, Y. Li, M. Jin, Z. Suo, The action of Pt in bimetallic Au–Pt/CeO_2 catalyst for water–gas shift reaction, Catalysis Today 158 (2010) 324–328.
[40] K.-r. Hwang, S.-k. Ihm, J.-s. Park, Enhanced CeO_2-supported Pt catalyst for water–gas shift reaction, Fuel Processing Technology 91 (2010) 729–736.
[41] P. Panagiotopoulou, J. Papavasiliou, G. Avgouropoulos, T. Ioannides, D.I. Kondarides, Water–gas shift activity of doped Pt/CeO_2 catalysts, Chemical Engineering Journal 134 (2007) 16–22.
[42] X. Tang, J. Chen, X. Huang, Y. Xu, W. Shen, $Pt/MnO_x–CeO_2$ catalysts for the complete oxidation of formaldehyde at ambient temperature, Applied Catalysis B: Environmental 81 (2008) 115–121.
[43] P. Lakshmanan, L. Delannoy, V. Richard, C. Méthivier, C. Potvin, C. Louis, Total oxidation of propene over $Au/xCeO_2–Al_2O_3$ catalysts: influence of the CeO_2 loading and the activation treatment, Applied Catalysis B: Environmental 96 (2010) 117–125.
[44] L.F. Liotta, M. Ousmane, G. Di Carlo, G. Pantaleo, G. Deganello, G. Marcì, L. Retailleau, A. Giroir-Fendler, Total oxidation of propene at low temperature over $Co_3O_4–CeO_2$ mixed oxides: role of surface oxygen vacancies and bulk oxygen mobility in the catalytic activity, Applied Catalysis A: General 347 (2008) 81–88.
[45] T. Masui, H. Imadzu, N. Matsuyama, N. Imanaka, Total oxidation of toluene on $Pt/CeO_2–ZrO_2–Bi_2O_3$/[gamma]-Al_2O_3 catalysts prepared in the presence of polyvinyl pyrrolidone, Journal of Hazardous Materials 176 (2010) 1106–1109.
[46] U. Oran, D. Uner, Mechanisms of CO oxidation reaction and effect of chlorine ions on the CO oxidation reaction over Pt/CeO_2 and Pt/CeO_2/[gamma]-Al_2O_3 catalysts, Applied Catalysis B: Environmental 54 (2004) 183–191.
[47] S. Damyanova, B. Pawelec, K. Arishtirova, M.V.M. Huerta, J.L.G. Fierro, The effect of CeO_2 on the surface and catalytic properties of $Pt/CeO_2–ZrO_2$ catalysts for methane dry reforming, Applied Catalysis B: Environmental 89 (2009) 149–159.
[48] A. Bueno-López, K. Krishna, M. Makkee, Oxygen exchange mechanism between isotopic CO_2 and Pt/CeO_2, Applied Catalysis A: General 342 (2008) 144–149.
[49] N. Goswami, D.K. Sharma, Structural and optical properties of unannealed and annealed ZnO nanoparticles prepared by a chemical precipitation technique, Physica E: Low-dimensional Systems and Nanostructures 42 (2010) 1675–1682.
[50] S. Wang, F. Gu, C. Li, H. Cao, Shape-controlled synthesis of $CeOHCO_3$ and CeO_2 microstructures, Journal of Crystal Growth 307 (2007) 386–394.
[51] A. Djelloul, M.S. Aida, J. Bougdira, F.T.I.R. Photoluminescence, X-ray diffraction studies on undoped and Al-doped ZnO thin films grown on polycrystalline [alpha]-alumina substrates by ultrasonic spray pyrolysis, Journal of Luminescence 130 (2010) 2113–2117.
[52] M.Y. Cui, X.Q. Yao, W.J. Dong, K. Tsukamoto, C.R. Li, Template-free synthesis of $CuO–CeO_2$ nanowires by hydrothermal technology, Journal of Crystal Growth 312 (2010) 287–293.
[53] M.L. Dos Santos, R.C. Lima, C.S. Riccardi, R.L. Tranquilin, P.R. Bueno, J.A. Varela, E. Longo, Preparation and characterization of ceria nanospheres by microwave-hydrothermal method, Materials Letters 62 (2008) 4509–4511.
[54] R. Wang, H. Xu, X. Liu, Q. Ge, W. Li, Role of redox couples of Rh_0/Rh[delta]+ and Ce^{4+}/Ce^{3+} in CH_4/CO_2 reforming over $Rh-CeO_2/Al_2O_3$ catalyst, Applied Catalysis A: General 305 (2006) 204–210.
[55] S. Damyanova, C.A. Perez, M. Schmal, J.M.C. Bueno, Characterization of ceria-coated alumina carrier, Applied Catalysis A: General 234 (2002) 271–282.
[56] P. Singh, M.S. Hegde, Controlled synthesis of nanocrystalline CeO_2 and $Ce_1–xMxO_2$-[delta] (M = Zr, Y, Ti, Pr and Fe) solid solutions by the hydrothermal method: structure and oxygen storage capacity, Journal of Solid State Chemistry 181 (2008) 3248–3256.
[57] A.M. Duarte de Farias, A.P.M.G. Barandas, R.F. Perez, M.A. Fraga, Water–gas shift reaction over magnesia-modified Pt/CeO_2 catalysts, Journal of Power Sources 165 (2007) 854–860.
[58] A.A. Barresi, G. Baldi, Deep catalytic oxidation of aromatic hydrocarbon mixtures: reciprocal inhibition effects and kinetics, Industrial & Engineering Chemistry Research 33 (1994) 2964–2974.
[59] J.J. Spivey, Complete catalytic oxidation of volatile organics, Industrial & Engineering Chemistry Research 26 (1987) 2165–2180.
[60] V. Balcaen, R. Roelant, H. Poelman, D. Poelman, G.B. Marin, TAP study on the active oxygen species in the total oxidation of propane over a $CuO–CeO_2$/[gamma]-Al_2O_3 catalyst, Catalysis Today 157 (2010) 49–54.